scientific reports

Check for updates

OPEN

A specific dispiropiperazine derivative that arrests cell cycle, induces apoptosis, necrosis and DNA damage

Victor P. Liu[1], Wai-Ming Li[1], Jack Lofroth[1], Mehreen Zeb[1], Brian O. Patrick[2], Tina M. Bott[3] & Chow H. Lee[1]✉

Dispiropiperazine compounds are a class of molecules known to confer biological activity, but those that have been studied as cell cycle regulators are few in number. Here, we report the characterization and synthesis of two dispiropiperazine derivatives: the previously synthesized spiro[2′,3]-bis(acenaphthene-1′-one)perhydrodipyrrolo-[1,2-a:1,2-d]-pyrazine (SPOPP-3, 1), and its previously undescribed isomer, spiro[2′,5′]-bis(acenaphthene-1′-one)perhydrodipyrrolo-[1,2-a:1,2-d]-pyrazine (SPOPP-5, 2). SPOPP-3 (1), but not SPOPP-5 (2), was shown to have anti-proliferative activity against a panel of 18 human cancer cell lines with IC_{50} values ranging from 0.63 to 13 μM. Flow cytometry analysis revealed that SPOPP-3 (1) was able to arrest cell cycle at the G2/M phase in SW480 human cancer cells. Western blot analysis further confirmed the cell cycle arrest is in the M phase. In addition, SPOPP-3 (1) was shown to induce apoptosis, necrosis, and DNA damage as well as disrupt mitotic spindle positioning in SW480 cells. These results warrant further investigation of SPOPP-3 (1) as a novel anti-cancer agent, particularly for its potential ability to sensitize cancer cells for radiation-induced cell death, enhance cancer immunotherapy, overcome apoptosis-related drug resistance and for possible use in synthetic lethality cancer treatments.

The use of chemicals and radiation to induce DNA damage is the most commonly used method for cancer therapy. Recently, there is an increased interest in manipulating the cell cycle to induce mitotic catastrophe as a novel anti-cancer therapeutic strategy[1–5]. Mitotic catastrophe is characterized by cells which would normally be arrested in G2/M phase due to damage in DNA or mitotic spindle but falsely proceed to mitosis due to defective cell cycle checkpoints[6]. The end result is senescence or cell death via either apoptosis, necrosis or autophagy[7]. This strategy relies on the use of DNA damaging agents or radiation in combination with cell cycle checkpoint inhibitors. Indeed, several G2/M phase checkpoint inhibitors[1–5], including irinotecan, a currently used chemotherapeutic drug for metastatic colorectal cancer, have shown potential to sensitize tumor cells to ionizing radiation. As such, the discovery of new compounds which cause G2/M cell cycle arrest remains an important area of cancer research[8–10].

There are currently few known biologically active dispiropiperazine derivatives. One of which is prospidium chloride. This compound, also known as prospidine, has cytostatic, anti-inflammatory and immuno-suppressive properties[11–13]. It has been classified as an anti-neoplastic compound based on its ability to inhibit T and B cell mitogenesis during lymphoblastic transformation[11], and to lower tumor volumes of carcinogen-induced mammary tumors in rats[12]. Currently, prospidium chloride is used as an anti-rheumatic drug in refractory rheumatoid arthritis[14].

Despite previous reports of biologically active dispiropiperazine compounds, other chemical derivatives have not been sufficiently explored. Here, we report for the first time the anti-proliferative activity of spiro[2′,3]-bis(acenaphthene-1′-one)perhydrodipyrrolo-[1,2-a:1,2-d]-pyrazine (SPOPP-3, **1**), a previously synthesized dispiropiperazine derivative. SPOPP-3 (**1**) has anti-proliferative activity against a panel of human cancer cell lines and is capable of arresting cell cycle at G2/M phase, and inducing apoptosis, necrosis and DNA damage as well as disrupting mitotic spindle positioning.

[1]Department of Chemistry and Biochemistry, Faculty of Science and Engineering, University of Northern British Columbia, Prince George, BC V2N 4Z9, Canada. [2]Department of Chemistry, University of British Columbia, Vancouver, BC V6T 1Z1, Canada. [3]Department of Physical Sciences, MacEwan University, 10700-104 Avenue, Edmonton, AB T5J 4S2, Canada. ✉email: chow.lee@unbc.ca

Results

Synthesis of SPOPP-3 (1) and SPOPP-5 (2). A recent report demonstrated the synthesis of two dispiropiperazine derivatives, spiro[2′,3]-bis(acenaphthene-1′-one)perhydrodipyrrolo-[1,2-a:1,2-d]-pyrazine (referred to here as SPOPP-3, **1**) and spiro[2′,5]-bis(acenaphthene-1′-one)perhydrodipyrrolo-[1,2-a:1,2-d]-pyrazine, through an azomethine ylide cycloaddition reaction using acenaphthenequinone (AcQ) and L-proline as substrates[15]. We performed a similar reaction with slight modifications as described in "Materials and methods" to obtain SPOPP-3 (**1**) (Fig. 1). Surprisingly, we also obtained a small quantity of spiro[2′,5′]-bis(acenaphthene-1′-one)perhydrodipyrrolo-[1,2-a:1,2-d]-pyrazine (referred to here as SPOPP-5, **2**) (Fig. 1 and Supplementary Figs. S2, S3, S6–S11), an isomer which has not been previously isolated due to its predicted unfavorable formation pathway[15,16]. Herein, we report for the first time, the purity (Supplementary Fig. S2) and structure of SPOPP-5 (**2**) as determined by FTIR (Supplementary Fig. S3), NMR (Supplementary Figs. S6–S10) and X-ray diffraction analyses (Supplementary Fig. S11).

SPOPP-3 (1) reduced cell viability in human cancer cell lines. To our knowledge, no bioactivity has been reported for SPOPP-3 (**1**). Herein, we show for the first time that SPOPP-3 (**1**) significantly reduced cell viability in human colon cancer cells (Fig. 2). For SPOPP-3 (**1**), the IC_{50} was 5.06 ± 1.43 μM, 5.42 ± 0.96 μM and 2.44 ± 0.83 μM in SW480, HT29 and HCT116 human colon cancer cells respectively (Table 1). In contrast, its isomer SPOPP-5 (**2**) had no significant effect, with IC_{50} > 100 μM (Fig. 2; Table 1). To determine whether SPOPP-3 (**1**) and SPOPP-5 (**2**) have different effects on different types of cancer cells, we assessed them on an additional 15 human cancer cell lines comprising another 8 different types of human cancers. Doxorubicin was used as a positive control on the cell lines and the summary is shown in Table 1. SPOPP-3 (**1**) remains inhibitory with IC_{50} values ranging from 0.63 ± 0.17 μM in human T lymphoblastoid cell line CEM to 13.0 ± 1.96 μM in human hepatoma cell line HepG2. Again, SPOPP-5 (**2**) showed insignificant activity in four additional cancer cell lines (MiaPaca-2, Panc-1, SKOV3 and MDA-MB-231) (Table 1). Based on the results that SPOPP-5 (**2**) had no significant anti-cell viability effect on 7 cancer cell lines, it was not further assessed on the other cell lines. The anti-proliferative effect of SPOPP-3 (**1**) was greatest against human leukemia cells lines (IC_{50} from 0.63 to 3.60 μM), human glioblastoma cell lines (IC_{50} from 2.95 to 6.30 μM), human colon cancer cell lines (IC_{50} from 2.44 to 5.42 μM), human cervical cancer cell lines (IC_{50} of 4.23 μM), human ovarian cancer cell lines (IC_{50} of 6.30 μM) and human breast cancer cell lines (IC_{50} from 4.00 to 6.17 μM). SPOPP-3 (**1**) has slightly weaker anti-proliferative activity against human liver cancer cell line (IC_{50} of 13.03 μM), human pancreatic cancer cell lines (IC_{50} from 8.62 to 9.17 μM) and human prostate cancer cell line (IC_{50} of 9.80 μM). Overall, the results showed that SPOPP-3 (**1**) has a relatively strong anti-proliferative effect on a panel of human cancer cell lines. To understand the mechanism whereby SPOPP-3 (**1**) exerts its anti-proliferative effect on cells, the following studies were conducted.

SPOPP-3 (1) arrested cell cycle at G2/M phase. To determine the mechanism whereby SPOPP-3 (**1**) decreases cell viability, flow cytometry was performed for cell cycle analysis. As shown in Fig. 3, treatment with 20 μM SPOPP-3 (**1**) caused cell cycle arrest in the G2/M phase (Fig. 3b). No activity was observed for SPOPP-5 (**2**). To further investigate whether SPOPP-3 (**1**) induces arrest at G2 or M phase, we performed Western blot analysis to detect phospho-histone H3, an established sensitive mitotic marker[17]. Indeed, phospho-histone H3 level was clearly increased in SW480 cells treated with SPOPP-3 (**1**) but not SPOPP-5 (**2**) (Fig. 4), indicating that SPOPP-3 (**1**) arrests SW480 cells at the M phase of the cell cycle. To further investigate the effects of SPOPP-3 (**1**) on the cell cycle, we performed immunofluorescence experiments to study cyclin B1 activation. Cyclin B1 is one of the key factors in controlling entry into mitosis[18,19] with its expression rapidly increased in G2 phase and peaking at late G2 or early M phase[20,21]. As shown in Fig. 5, the population of tetraploid cells in SPOPP-3 (**1**)-treated cells as indicated by cells having doubled DAPI signal, was significantly increased when compared with DMSO control. This confirms flow cytometry results that SPOPP-3 (**1**) caused cell cycle arrest in the G2/M phase where the cells failed to divide into daughter cells. In control cells, most of the tetraploid cells had significantly higher cyclin B1 staining compared to SPOPP-3-treated tetraploid cells (Fig. 5b). Thus, our results indicate that SPOPP-3 (**1**) treatment is associated with defective cyclin B1 activation.

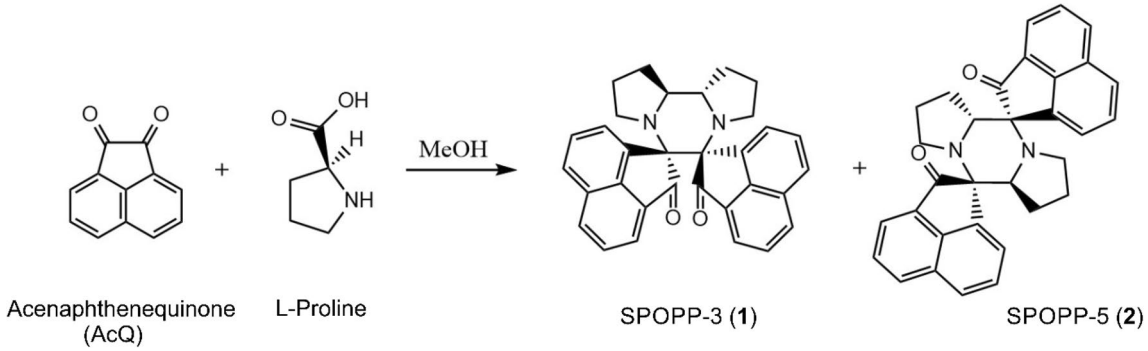

Figure 1. Synthesis of dispiropiperazine derivatives SPOPP-3 (**1**) and SPOPP-5 (**2**).

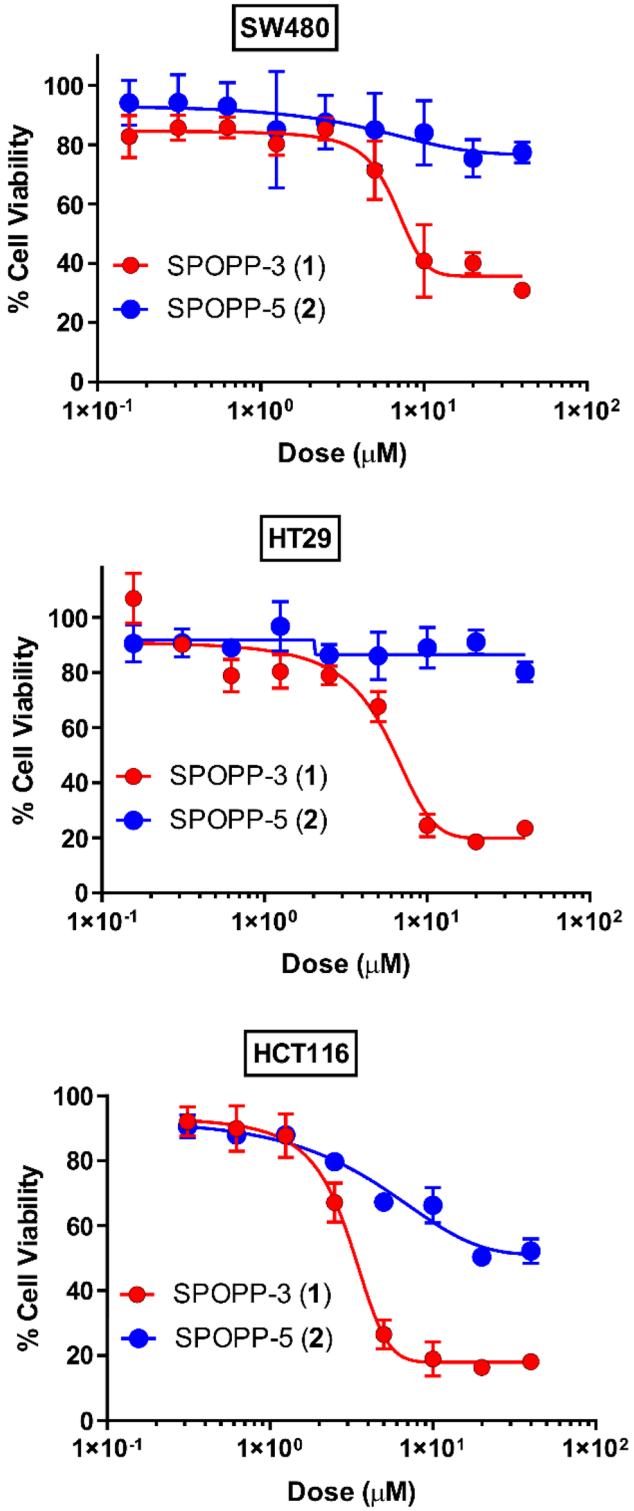

Figure 2. SPOPP-3 (**1**) inhibited human colon cancer cell viability. Cell viability in SW480, HT29 and HCT116 human colon cancer cells was assessed using the MTT assay. Cells were treated with different concentrations of SPOPP-3 (**1**) or SPOPP-5 (**2**) for 48 h. Results shown are representative from three separate experiments. Error bars are SEM.

SPOPP-3 (1), but not SPOPP-5 (2), induced cell apoptosis and necrosis. To determine the possible effect of SPOPP-3 (**1**) on cell death that led to the observed decrease in cell viability, we used flow cytometry

Cell lines	Types	IC_{50} (μM) of compounds		
		SPOPP-3 (1)	SPOPP-5 (2)	Doxorubicin
SW480	Human colon cancer	5.06 ± 1.43	> 100	0.22 ± 0.16
HT29	Human colon cancer	5.42 ± 0.96	> 100	0.26 ± 0.02
HCT116	Human colon cancer	2.44 ± 0.83	> 100	0.10 ± 0.05
MiaPaca2	Human pancreatic cancer	8.62 ± 3.18	> 100	0.25 ± 0.24
Panc1	Human pancreatic cancer	9.17 ± 2.67	> 100	0.43 ± 0.14
SKOV3	Human ovarian cancer	6.30 ± 1.35	> 100	0.04 ± 0.01
MDA-MB-231	Human breast cancer	6.17 ± 1.84	> 100	1.06 ± 0.03
MCF-7	Human breast cancer	5.76 ± 0.10	ND	0.03 ± 0.02
MCF-7-Adr	Human breast cancer	4.00 ± 0.85	ND	ND
T47D	Human breast cancer	4.76 ± 1.24	ND	ND
HepG2	Human liver cancer	13.03 ± 1.96	ND	0.36 ± 0.12
HeLa	Human cervical cancer	4.23 ± 1.29	ND	0.26 ± 0.12
DU145	Human prostate cancer	9.80 ± 1.94	ND	0.02 ± 0.01
K562	Human leukemia	3.60 ± 1.13	ND	ND
KG1a	Human leukemia	1.76 ± 0.84	ND	ND
CEM	Human leukemia	0.63 ± 0.17	ND	ND
U251	Human glioblastoma	2.95 ± 0.09	ND	0.01 ± 0.004
U87	Human glioblastoma	6.30 ± 1.72	ND	0.01 ± 0.002

Table 1. IC_{50} of SPOPP-3 (**1**), SPOPP-5 (**2**) and doxorubicin against human cancer cell lines. The IC_{50} the data shown is an average taken from three independent experiments. *ND* not determined.

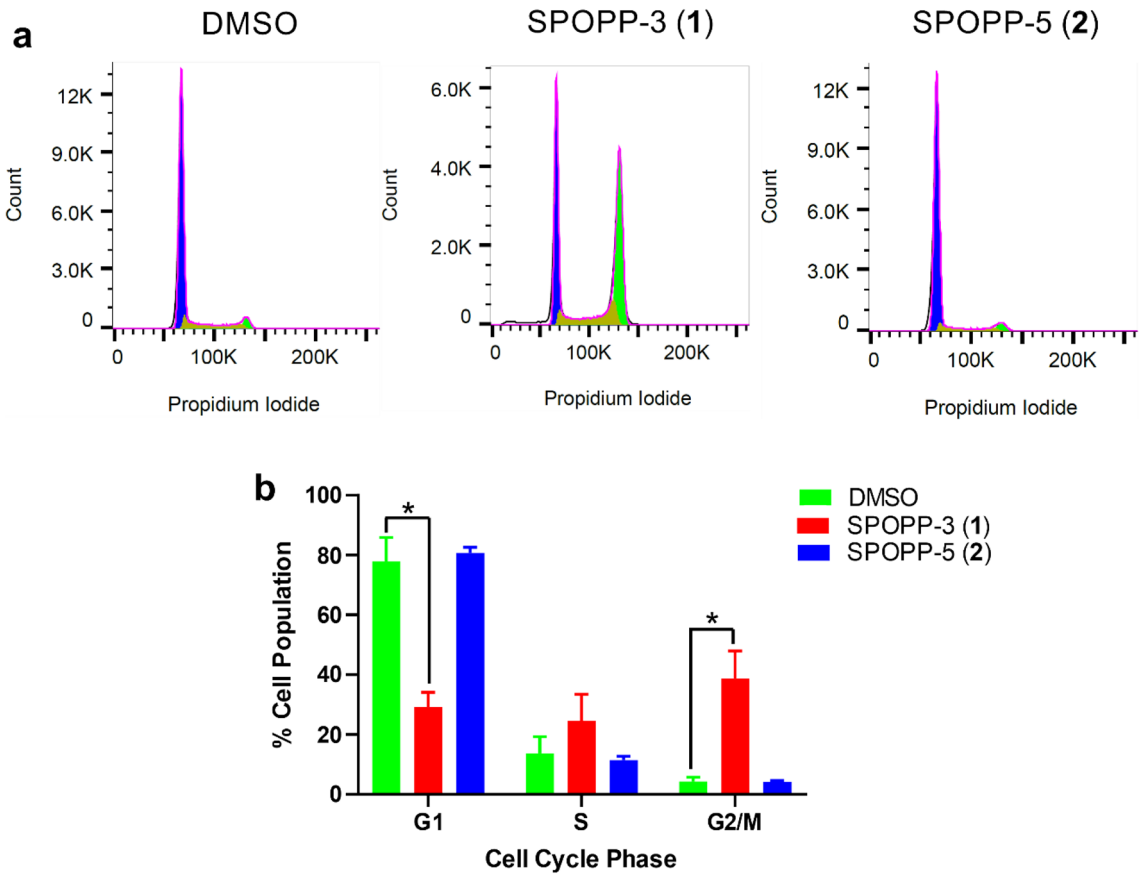

Figure 3. SPOPP-3 (**1**) arrested cell cycle at G2/M phase in SW480 cells. (**a**) SW480 cells were treated with 2% DMSO, 20 μM SPOPP-3 (**1**), or 20 μM SPOPP-5 (**2**) for 24 h after which cells were harvested and subjected to cell cycle analysis using flow cytometry. (**b**) The results from (**a**) and two another additional biological replicates (n = 3) were combined and expressed as shown. The cell cycle percentages were calculated based on the Watson Pragmatic model. Two-way ANOVA was performed: *p < 0.0001.

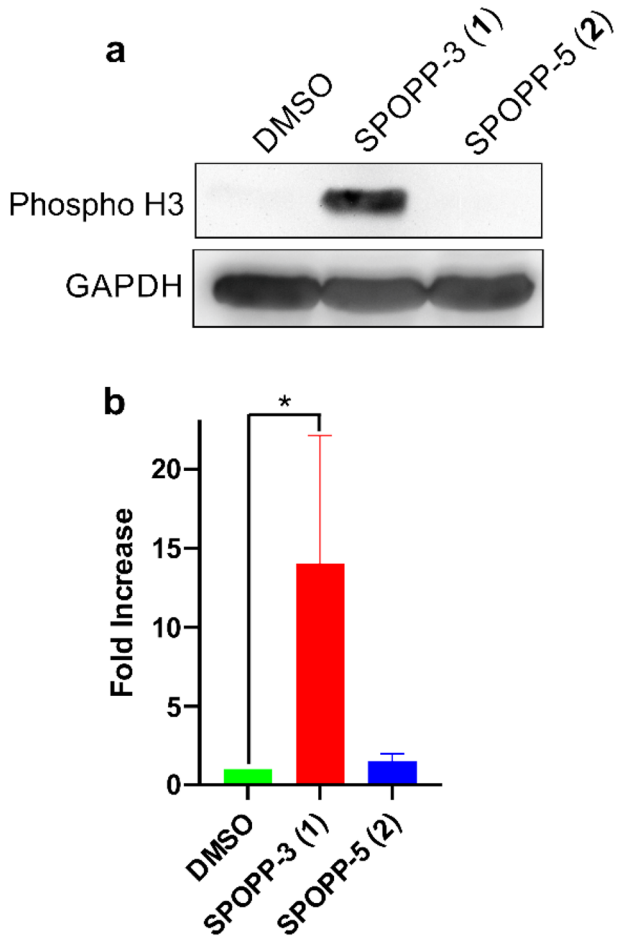

Figure 4. SPOPP-3 (**1**) induced phospho-histone H3 in SW480 cells. (**a**) Immunoblots showing phospho-histone H3 and GAPDH expression upon treatment with 2% DMSO, 20 µM SPOPP-3 (**1**) or 20 µM SPOPP-5 (**2**) for 24 h. (**b**) The results from (A) and another two biological replicate (n = 3) were averaged and expressed as shown. t-test was used: *p < 0.05.

to analyse apoptosis and necrosis. The commonly used stains to detect necrosis and apoptosis are 7-AAD and Annexin V-PE, respectively. After treatment with SPOPP-3 (**1**), SPOPP-5 (**2**) or 2% DMSO for 24 h, cells were double stained with 7-AAD and Annexin V-PE. As shown in Fig. 6a, cells treated with SPOPP-3 (**1**) changed to a more necrotic state (Q1; 32.64%) as compared to the DMSO-treated cells (Q1; 0.5%), and this is statistically significant (Fig. 6b). SPOPP-3 (**1**) also significantly induced apoptosis (Q2 + Q4) in SW480 cells (Fig. 6). On the other hand, SPOPP-5 (**2**) had no significant effect on apoptosis or necrosis as compared to the control.

Effect of SPOPP-3 (1) on mitotic spindle formation. Immunofluorescence studies were carried out to investigate the potential function of SPOPP-3 (**1**) as a microtubule toxin. Two drugs, vinblastine and colchicine which are well known to disrupt microtubules, were used as positive controls. Vinblastine, which belongs to the family of vinca alkaloids, binds to tubulin at a specific site and inhibits mitotic spindle formation leading to cell cycle disruption[22,23]. When used at high concentrations, vinblastine is known to cause paracrystal formation due to tightly packed tubulin aggregates[24]. Indeed, when SW480 cells were treated with 50 nM vinblastine, paracrystals were observed (Fig. 7). Colchicine, on the other hand, disrupted microtubules and caused diffuse α-tubulin staining throughout the cells (Fig. 7). In contrast, mitotic spindles could be observed in cells treated with SPOPP-3 (**1**). However, the positions of the mitotic spindles appeared to be disrupted when compared with control cells treated with DMSO (Fig. 7). Displacement of the mitotic spindles was also associated with the lack of chromosome alignment at the equator of the cell (Fig. 7). In summary, these results suggest that although SPOPP-3 (**1**) does not disrupt microtubule formation, mitotic spindle positioning appears to be affected.

SPOPP-3 (1) induced DNA damage. Based on the findings that SPOPP-3 (**1**) causes G2/M arrest associated with cyclin B1 down regulation and mitotic spindle displacement, it may be possible that the activity of SPOPP-3 (**1**) is via DNA damage[19,25]. To investigate this possibility, we used the qPCR-based method (LORD-Q) to detect DNA lesions[26]. Since this method can detect DNA damage regardless of the type of DNA lesion, we reason that this is the most appropriate method. As shown in Fig. 8, although the data did not reach statistical

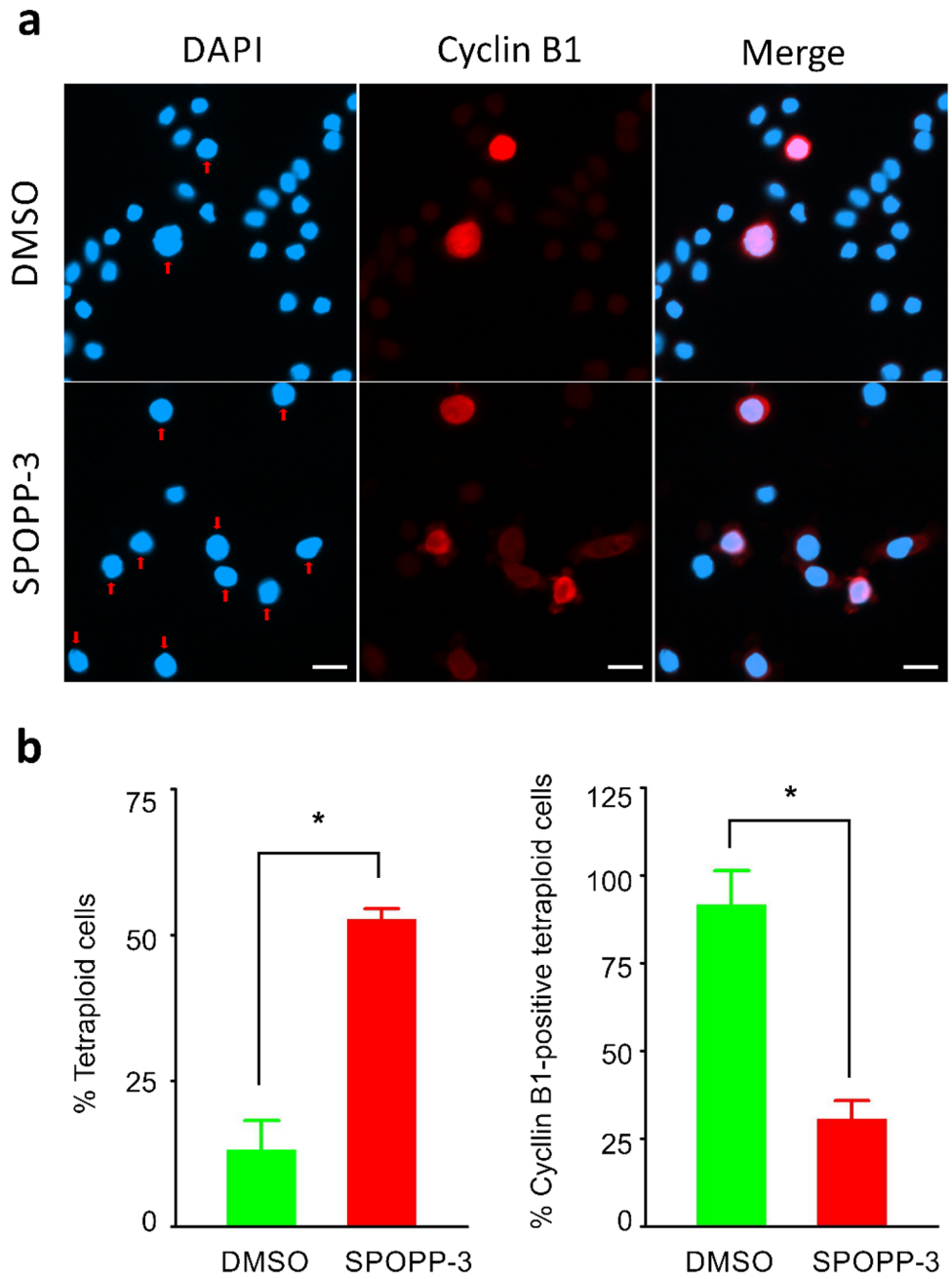

Figure 5. Defective cyclin B1 induction in SPOPP-3 treated cells as shown by immunofluorescence experiments. SW480 cells were treated with 40 μM SPOPP-3 or 2% DMSO for 24 h before fixation and immunostaining with cyclin B1 antibody and DAPI. (**a**) Representative image of cells treated with SPOPP-3 (lower images) showing a large population of tetraploid cells (indicated by arrows) without cyclin B1 staining. In contrast, DMSO-treated cells have a relatively small population of tetraploid cells all of which expressed cyclin B1. (**b**) Tetraploid cells (with doubled DAPI signal) (left) and the percentage of tetraploid cells positive for cyclin B1 (right) were quantified in each group and presented as average ± SD. One-way ANOVA was used: *$p < 0.05$. Scale bar 20 mm.

significance because of the large variation in data, the effect of SPOPP-3 (**1**) on DNA damage can be detected as early as 1 h after treatment. However, such effect was much reduced after 20 h of treatment (Fig. 8).

Discussion

In this study, we report the synthesis of SPOPP-3 (**1**) and show for the first time that it has strong anti-proliferative activity against 18 human cancer cell lines (Table 1). To our surprise, using the previously reported synthesis procedure[15,16], we also obtained the structural isomer SPOPP-5 (**2**), a novel compound. We believe

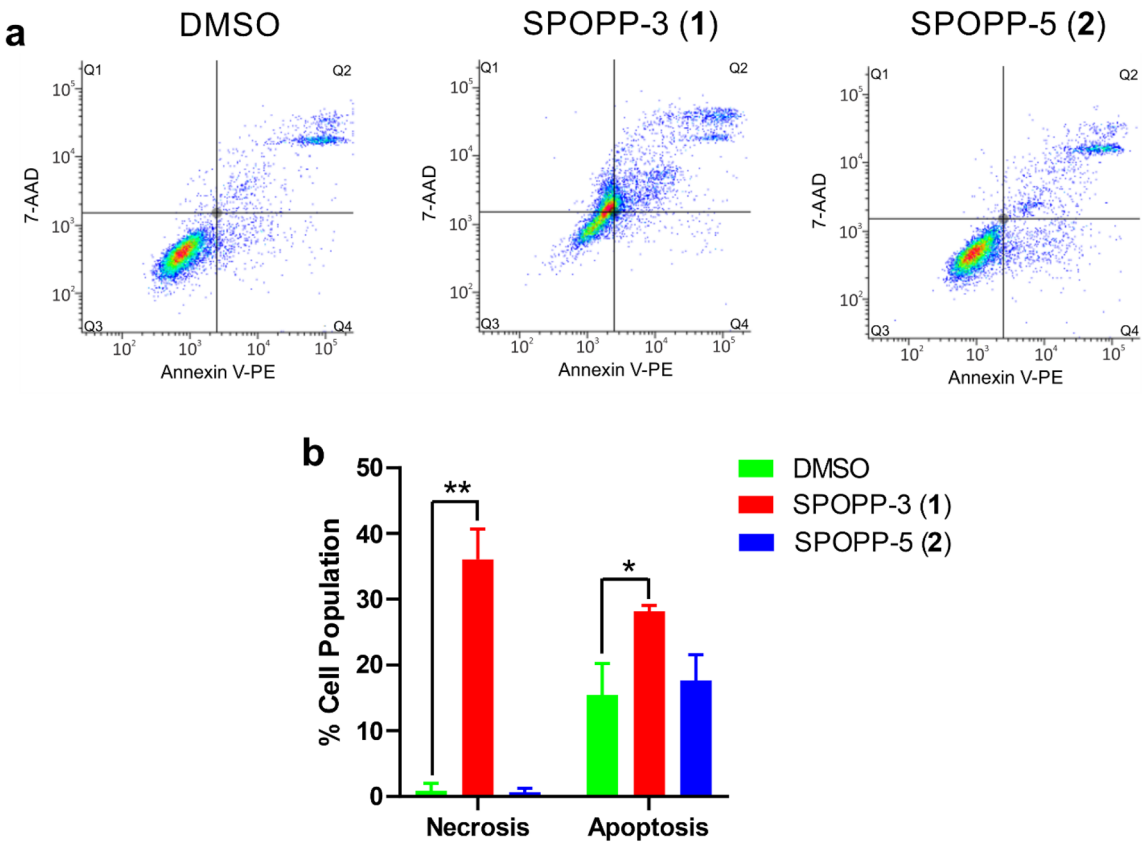

Figure 6. SPOPP-3 (**1**) induced apoptosis and necrosis in SW480 cells. (**a**) SW480 cells were treated with 2% DMSO, 20 μM SPOPP-3 (**1**), or 20 μM SPOPP-5 (**2**) for 24 h, after which cell lysates were isolated and subjected to cell death analysis using flow cytometry. (**b**) The results from (**a**) and two other additional biological replicates (n = 3) were combined and expressed as shown. Two-way ANOVA was used: *$p < 0.005$, **$p < 0.0001$.

that SPOPP-5 (2) was formed in our hands because we used 35 °C and 3 h for the synthesis whereas Haddad et al.[15] refluxed their synthesis reaction at 65 °C for 2 h. Lower synthesis temperature during cycloaddition reactions is known to favor more kinetically controlled product[16]. In contrast to SPOPP-3 (**1**), SPOPP-5 (**2**) had virtually no anti-proliferative activity (Table 1). We speculate that the configuration of the two carbonyl groups in SPOPP-3 (**1**), specifically in the absence of additional chemical components in between them, may contribute to its anti-proliferative activity (Fig. 1). Future structure–activity relationship studies would need to be conducted to test this hypothesis. The differential effect of SPOPP-3 on the different cancer cell lines could be related to the growth rate of the cell lines. For example, SPOPP-3 has stronger anti-proliferative effect on the faster growing human leukemia cell lines (K562, KG1a, CEM) and glioblastoma cell lines (U251, U87) but has weaker effect on the slower growing HepG2 liver cancer cell line, DU145 prostate cancer cell line, and pancreatic cancer cell lines (MiaPaca2, Panc1) (Table 1). Interestingly, this is not true for the positive control doxorubicin which showed strong anti-proliferative effect on both faster growing cells (U251, U87) and slower growing cells (DU145, SKOV3). Such observations suggested that SPOPP-3 and doxorubicin exerted their anti-proliferative effect through different mechanisms.

The anti-proliferative activity of SPOPP-3 (**1**) was associated with its ability to induce apoptosis and necrosis (Fig. 6), as well its ability to cause cell cycle arrest in the G2/M phase (Fig. 3). Using phosphorylated histone H3 as an M phase marker, it was shown that at least some cells were arrested in M phase (Fig. 4). Our results also showed that cyclin B1 expression was drastically reduced upon SPOPP-3 (**1**) treatment (Fig. 5). Although a rise in cyclin B1 expression in late G2 phase and its translocation to the nucleus is important for the initiation of mitosis, its depletion using siRNA knockdown does not cause cells to be arrested only in G2 phase as this can be explained by the redundant function of cyclin B2[18,27]. We also demonstrated using microscopy that while microtubules seem to be unaffected by SPOPP-3 (**1**) treatment, defects in the M phase including mitotic spindle positioning and condensed chromosome alignment, were observed (Fig. 7). This may be due to decreased cyclin B1 levels as it is known that cyclin B1 is normally recruited to centrosomes and kinetochores[28,29]. We further investigated whether SPOPP-3 (**1**) causes DNA damage as it has been documented that cyclin B1 levels are reduced as a result of DNA damage[30,31]. Indeed, our results suggest that similar to bleomycin[26], Indeed, our results show that SPOPP-3 (**1**) causes DNA damage at an early stage which was detectible at 1 h but not at 20 h after treatment (Fig. 8). This is similar to the effect of bleomycin[26] and is likely the result of the quick DNA damage repair response [32]. As a consequence, such an early DNA damage event could lead to cyclin B1 reduction, cell cycle arrest, apoptosis and necrosis which are cellular processes that occur much later.

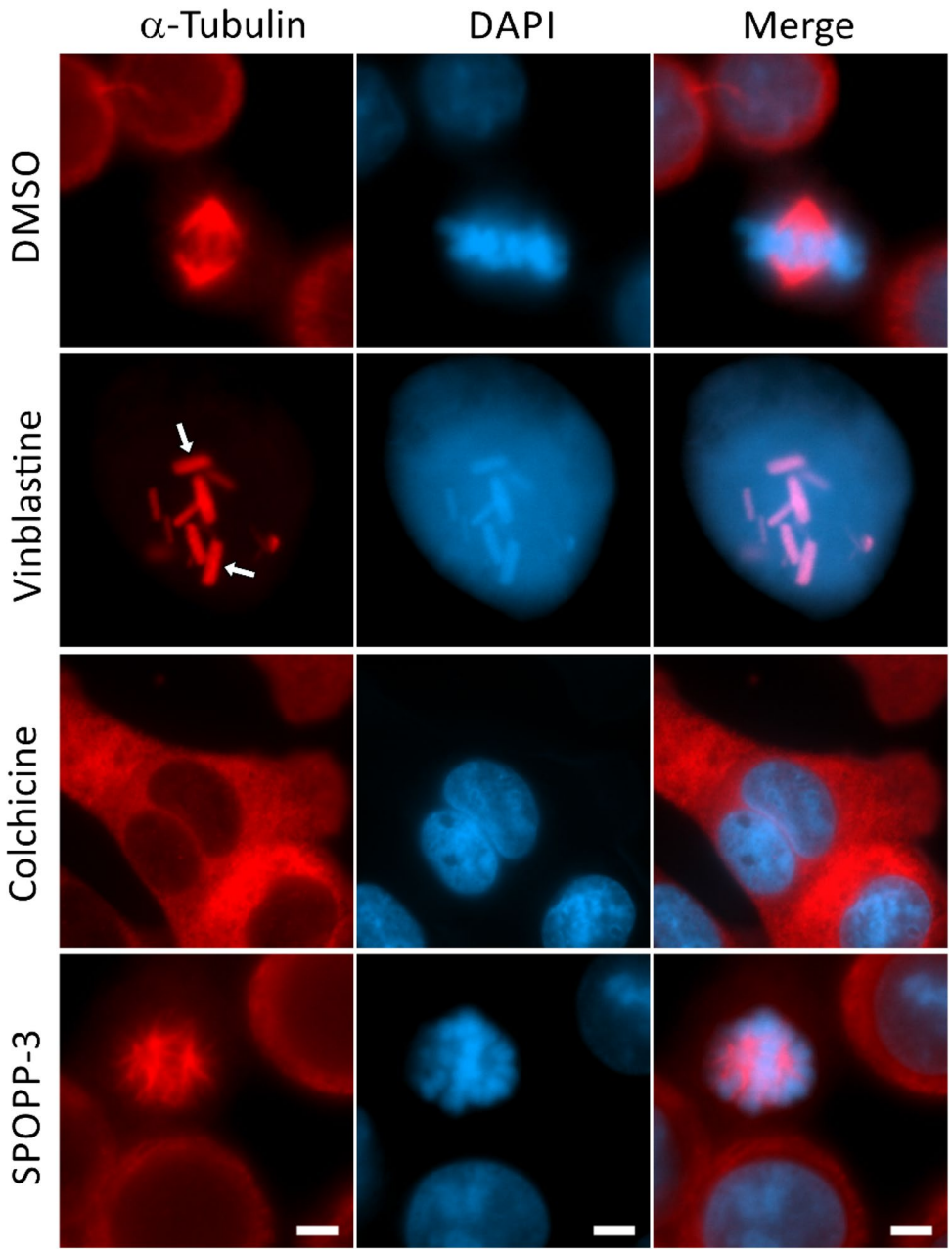

Figure 7. SPOPP-3 (**1**) does not cause microtubule disruption. SW480 cells were treated with 50 nM vinblastine, 1 μM colchicine or 40 μM SPOPP-3 (**1**) for 24 h before fixation and immunostaining with α-tubulin antibody and DAPI. Mitotic spindles were clearly observed in SPOPP-3 (**1**) treated cells while colchicine and vinblastine induced microtubule disruption via different mechanisms. Diffuse α-tubulin staining in the cytoplasm and para-crystal formation (arrows) can be observed with colchicine and vinblastine treatment respectively. Scale bar 5 mm.

The anti-proliferative properties of SPOPP-3 (**1**) has important implications in cancer therapy. Synthetic lethality is a novel approach in cancer treatment[4,5]. Since SPOPP-3 (**1**) is a potent inducer of G2/M arrest, it has the potential to be used in combination with G2/M checkpoint inhibitors to trigger mitotic catastrophe which is currently viewed as a favorable treatment strategy to enhance cell death either via apoptosis, necrosis or autophagy[1–5]. Particularly, in most of melanoma cases where G1/S transition mediated by the cyclin-CDK4 pathway is defective and has increased dependence on the G2/M checkpoint to induce cell cycle arrest when exposed to DNA damage, SPOPP-3 (**1**) may have an added advantage in combination with G2/M inhibitors[4]. Secondly, we found that SPOPP-3 (**1**) is an inducer of necrosis. Several lines of investigations have provided evidence to support the role of necrosis in enhancing cancer immunotherapy and as a possible strategy to overcome the resistance of cancer cells to apoptosis[33,34]. To this end, it will be important to assess whether SPOPP-3 (**1**) has such prowess in inducing pro-inflammatory processes by means of releasing damage-associated molecular

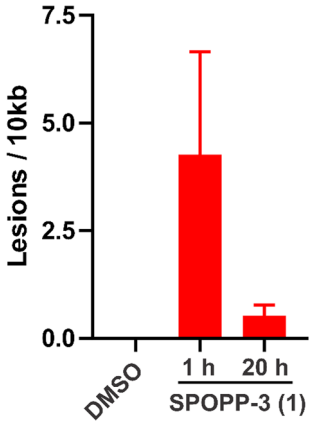

Figure 8. SPOPP-3 (**1**) induced DNA damage. DNA lesion quantification using LORD-Q in SW480 cells treated with 40 μM SPOPP-3 (**1**) for the indicated time periods. Short and long amplicons amplified from the mtDNA gene was used in the quantification of lesions in mitochondrial DNA. Data presented are averaged from three biological replicates ± SEM (n = 3).

patterns such as high mobility group 1 (HMGB1) protein, a marker for necrosis. Release of such factors into the extracellular matrix may lead to activation of CD8+ leukocytes and promote anti-tumor immunity[34].

It is also important to decipher further the mechanism whereby SPOPP-3 (**1**) arrests cells at G2/M phase. For instance, piperazine derivatives have been shown to generate reactive oxygen species (ROS) within cells[35]. Therefore, it would be of interest to investigate whether SPOPP-3 (**1**) can generate ROS leading to oxidative DNA damage and subsequent arrest at G2/M phase. In terms of necrosis, one of the modes of cell death detected in cells treated with SPOPP-3 (**1**), it has become increasingly clear that necrosis may not simply be an uncontrolled cellular process, but rather a regulated pathway commonly known as necroptosis[36]. Necroptosis has also been reported to increase cancer metastasis in certain cell lines[37]. The duality of necroptosis being anti- and pro-tumorigenic still requires investigation to determine in what context is necroptosis beneficial. Since we have found respectable anti-proliferative activity of SPOPP-3 (**1**) against a large panel of cancer cell lines, it would be integral to further study the mode of cell death in different cell lines.

In conclusion, we describe the synthesis and biochemical characterization of a specific dispiropiperazine derivative called SPOPP-3 (**1**) with strong anti-proliferative activity against a wide panel of human cancer cell lines. SPOPP-3 (**1**) is able to induce DNA damage, apoptosis, necrosis, arrests cell cycle at G2/M phase and disrupts normal mitotic spindle positioning. This study has laid the foundation for the further development of SPOPP-3 (**1**) for possible use as a chemical tool to perturb and understand cellular processes, as well as a potential anti-cancer compound. For the latter, SPOPP-3 (**1**) should be explored in synthetic lethality approach and as a necrosis-inducing anti-cancer compound.

Methods and materials

Synthesis and purification of SPOPP-3 (1) and SPOPP-5 (2). We adopted the previously described method for synthesizing spiro[2′,3]-bis(acenaphthene-1′-one)perhydrodipyrrolo-[1,2-a:1,2-d]-pyrazine (SPOPP-3, **1**)[15,16]. A mixture of acenaphthenequinone (1.822 g, 10 mmol) and L-proline (1.151 g, 10 mmol; Sigma-Aldrich) were dissolved in methanol (200 mL) and heated at 35 °C for 3 h. The reaction was monitored by thin layer chromatography (TLC) using ethyl acetate:hexane (1:2; v/v), and the spots were visualized using UV light (254 nm). Typically, an orange precipitate was formed during the first hour which changed to an orange-brown color after an additional hour and to a dark brown color after completion of the reaction. Solvent was removed under reduced pressure leaving a dark brown powder (1.722 g). Crude product, containing both SPOPP-3 (**1**) and SPOPP-5 (**2**), was mixed with 2 g of normal silica in 200 mL methanol. Solvent was removed under reduced pressure and the silica mixture was dry-loaded onto a column. Purification by flash chromatography, using normal-phase silica (50 g) and a 9:1 mixture of hexanes and ethyl acetate at a flow rate of 12 mL/min, was used to isolate a mixture of SPOPP-3 (**1**) and SPOPP-5 (**2**). Subsequent purification with three runs of flash chromatography employing a total of 686 mg of crude product were conducted. An orange-coloured band eluting at 530–830 mL corresponding to Rf = 0.14 with 9:1 (hexanes:ethyl acetate) was dried under reduced pressure to produce 280 mg of semi-purified SPOPP-3 (**1**). SPOPP-3 (**1**) was subsequently purified for biological testing by HPLC using a Phenomenex Luna 5u Phenyl-Hexyl 4.60 mm × 250 mm column. A gradient from 80 to 92% acetonitrile for 6 min at a flow rate of 2 mL/min was used as the eluent conditions. For the semi-purified SPOPP-3 (**1**), a total of 12.5 mg was injected into the HPLC and 5 mg (16%) of purified SPOPP-3 (**1**) (at retention of 4.08 min) was obtained. A yellow-coloured band eluting at 320–405 mL corresponding to Rf = 0.24 (9:1 hexanes:ethyl acetate) produced 120 mg of purified SPOPP-5 (**2**). SPOPP-5 (**2**) was purified using the same HPLC conditions as SPOPP-3 (**1**). One hundred twenty mg of semi-purified SPOPP-5 (**2**) was injected into HPLC and 21 mg (3%) of purified SPOPP-5 (**2**) (at retention of 6.02 min) was obtained. HPLC–MS and NMR analyses were used to confirm the identity of SPOPP-3 (**1**) and SPOPP-5 (**2**). 1D and 2D NMR spectra were recorded on an Agilent/Varian Inova 400 MHz NMR spectrometer with a 5 mm Kimble NMR tube (Rockwood,

TN, USA) at the University of Alberta or on a Bruker 600 MHz NMR with a cryoprobe at the University of British Columbia. All HPLC analyses were performed on Agilent 1260 Infinity Systems with UV detector, and mass spectrometry were done using Agilent 6120 Single Quad MS.

X-ray crystallographic analysis. Single orange irregular crystals of SPOPP-5 (**2**) (50 mg) were recrystallized from acetonitrile (10 mL) by slow evaporation. Crystals were obtained on day 7. A suitable crystal with dimensions $0.22 \times 0.20 \times 0.11$ mm^3 was selected and mounted on a Bruker APEX II area detector diffractometer. The crystal was kept at a steady $T = 90(2)$ K during data collection. The structure was solved with the ShelXT[38] solution program using dual methods and Olex2[39] as the graphical interface. The model was refined with XL[38] using full matrix least squares minimization on F^2.

Cell culture. All cell lines were obtained from American Type Culture Collection except HT29 (colon adenocarcinoma) which was obtained from Dr. Ranjana Bird at UNBC. All cells were maintained in Eagle's Minimal Essential Medium (Lonza) except the following: MiaPaca-2 and Panc-1 were maintained in Dulbecco's Modified Eagle Medium (Lonza), while K562, KG1a and CEM were maintained in RPMI 1640 medium (Lonza). All media were supplemented with 10% fetal bovine serum (Life Technologies Inc.) and antibiotics.

Cell viability assay. The cytotoxic MTT assay was used to assess cell viability as previously described[40]. Briefly, cells were plated at a density of 1.5×10^3 cells/well in 96-well plates. After 24 h, cells were treated with SPOPP-3 (**1**) or SPOPP-5 (**2**) for 48 h with concentration range from 0.16 to 100 μM. Cells were treated with the positive control doxorubicin from 0.003 to 0.8 μM. All absorbance data were expressed relative to the control, 0.1% DMSO, taken as 100% cell viability.

Preparation of cell lysates, immunoblot analysis and antibodies. SW480 cells were seeded in 6-well plates at a density of 3.0 x 10^5 cells per well and then treated on the next day with 20 μM SPOPP-3 (**1**), 20 μM SPOPP-5 (**2**), or 2% DMSO for 24 h. Cell lysates were prepared as previously described[41]. For immunoblot analysis, protein samples were resolved on a 10% SDS-PAGE and transferred onto a nitrocellulose membrane. The phospho H3 antibody (Ser10) (D2C8, 1:1,000, Cell Signaling) was used with an overnight incubation at 4 °C. Anti-GAPDH (G8795, clone GAPDH-71.1, 1:20,000, Sigma) was also used. Anti-mouse IgM-HRP (sc-2064, 1:4000, Santa Cruz Biotechnology), anti-mouse IgG-HRP (W402B, 1:4000, Promega) and anti-rabbit IgG-HRP (W401B, 1:4000, Promega) were used as secondary antibodies. All blots were visualized with the FluorChem Q system (ProteinSimple). Densitometry analysis was performed using the AlphaView Q software (ProteinSimple).

Flow cytometry apoptosis and cell cycle analyses. Cells were plated at 2.5×10^5 cells/well in 6-well plates and treated with compounds as described above. Cells were trypsinized followed by centrifugation and washed twice with phosphate-buffered saline. Live cells were stained with PE Annexin V and 7-AAD according to the manufacturer's instructions for Apoptosis Detection Kit I (BD Pharmingen) and analysed by flow cytometry using a BD FACSMelody cell sorter (BD Biosciences) and BD FACSChorus software (V 1.0). For cell cycle analysis, the BD cycletest plus DNA reagent kit was used to stain for DNA and the data was analysed using the software FlowJo.

Immunofluorescence. SW480 cells were plated in 4-well cover glass chambers at a density of 15×10^4 cells per well with 0.5 mL EMEM. The cells were treated with the indicated drugs for 24 h before fixation using 100% methanol (− 20 °C) for 10 min. Subsequently, the cells were blocked using PBS with 2% BSA and 0.1% Triton-x-100 and then stained with α-tubulin antibody (1:100; Ab4074; Abcam) or cyclin B1 antibody (D5C10, 1:200, cell signaling). Anti-mouse-AF594 and anti-rabbit-AF 594 (1:200; Molecular Probes) were used as secondary antibodies respectively. All antibodies used were diluted in PBS with 0.5% BSA and 0.1% Triton-x-100. All blocking and antibody incubation steps were conducted for 1 h at room temperature. After each antibody incubation step, the cells were washed 3 times (10 min each) with wash buffer containing 0.1% Triton-x-100 in PBS. For cyclin B1 immunofluorescence, cells were fixed in 4% paraformaldehyde for 15 min at room temperature. To stain for DNA, cells were incubated with DAPI dihydrochloride (300 nM diluted in PBS) for 5 min after immunostaining with the secondary antibody. All fluorescence images were taken using an inverted Zeiss Axio Observer Z1 microscope with a motorized stage, Zeiss Axiocam 503 mono camera, Colibri 2 multicolor LED light source, Plan-Apochromat 20×/0.8 M27 or Plan-Apochromat 63×/1.4 Oil DIC M27 as objectives. For the quantification of tetraploid cells, DAPI signal in each cell was quantified in each image using the region of interest function in the Zen software. Tetraploid cells were distinguished with a DAPI signal double that of the remaining cells in the same image. Three images (each with at least 36 cells) from each group were quantified. The population of tetraploid cells that were cyclin B1 positive was then determined in each image and presented as an average for each group. Vinblastine sulfate and colchicine (both purchased from Sigma) were included as positive controls for microtubule toxins.

DNA damage quantification. To assess whether SPOPP-3 treatment causes DNA damage, a long-run real-time PCR-based method (LORD-Q) was used with modifications[26]. SW480 cells (2.5×10^6) were treated in 6-well plates with DMSO (control) or 40 μM SPOPP-3 for the indicated time periods before being harvested for total DNA isolation using the DNeasy Blood and Tissue kit (Qiagen). LORD-Q method was carried out using the established primer sets for both the long and short amplicons for the mtDNA gene[26]. PCR efficiencies were

calculated using 37.5, 18.75, 9.375 and 4.688 ng DNA as template per PCR reaction. The rtPCR reaction (15 µL total volume) consisted of 0.05 × ResoLight dye, 1 × KAPA2G Fast Hot Start ReadyMix, 500 nM of forward and reverse primer, and the aforementioned quantities of isolated DNA as template. For amplification of short amplicons as reference, Quantabio PerfeCTa® SYBR® Green FastMix® was used. Real time PCR analysis was carried out using a Bio-Rad CFX96 system and data analysis was performed using CFX Maestro software. The number of lesions per 10 kb was calculated based on the previously established equation[26,42]. The data presented is averaged from 3 biological replicates ± S.E.M.

Statistical analysis. The cytotoxic MTT assays were performed in triplicate (3 wells/treatment) and the absorbance reading from the respective control was taken as 100% cell viability. For immunoblot analysis, the densitometry of phospho-histone H3 bands were normalized to their respective GAPDH bands and then expressed relative to the DMSO control (taken as 1.0). One-way or two-way ANOVA was performed as indicated. Data are expressed as mean ± SD and were analysed using GraphPad Prism version 8.0.2 (La Jolla, CA) or t-test. Holm-Sidak test was used for post-hoc analysis. A p value < 0.05 was considered statistically significant.

Data availability

The datasets used and/or analysed during the current study are available upon request from the corresponding author.

Received: 16 March 2023; Accepted: 25 May 2023
Published online: 29 May 2023

References

1. Visconti, R., Monica, R. D. & Grieco, D. Cell cycle checkpoint in cancer: A therapeutically targetable double-edged sword. *J. Exp. Clin. Cancer Res.* **35**, 153 (2016).
2. Dillon, M. T., Good, J. S. & Harrington, K. J. Selective targeting of the G2/M cell cycle checkpoint to improve the therapeutic index of radiotherapy. *Clin. Oncol.* **26**, 257–265 (2014).
3. Wang, Y. *et al.* Radiosensitization by irinotecan is attributed to G2/M phase arrest, followed by enhanced apoptosis, probably through the ATM/Chk/Cdc25C/Cdc2 pathway in P53-mutant colorectal cancer cells. *Int. J. Oncol.* **53**, 1667–1680 (2018).
4. Barnaba, N. & LaRocque, J. R. Targeting cell cycle regulation via the G2-M checkpoint for synthetic lethality in melanoma. *Cell Cycle* **20**, 1041–1051 (2021).
5. Nikolakopoulou, A. *et al.* G2/M checkpoint abrogation with selective inhibitors results in increased chromatid breaks and radiosensitization of 82–6 hTERT and RPE human cells. *Front. Pub. Health* **9**, 675095 (2021).
6. Galluzzi, L. *et al.* Molecular mechanisms of cell death: Recommendations of the Nomenclature Committee on cell death 2018. *Cell Death Differ.* **25**, 486–541 (2018).
7. Sazonova, E. V. *et al.* A link between mitotic defects and mitotic catastrophe: Detection and cell fate. *Biol. Direct.* **16**, 25 (2021).
8. Lu, W. J. *et al.* #2714, a novel active inhibitor with potent G2/M phase arrest and antitumor efficacy in preclinical models. *Cell Death Discov.* **4**, 24 (2018).
9. Wang, H. *et al.* Erianin induces G2/M-phase arrest, apoptosis, and autophagy via the ROS/J signaling pathway in human osteosarcoma cells in vitro and in vivo. *Cell Death Dis.* **7**, e2247 (2016).
10. Cabrera, M. *et al.* G2/M cell cycle arrest and tumor selective apoptosis of acute leukemia cells by a promising benzophenone thiosemicarbazone compound. *PLoS One* **10**, 10136878 (2015).
11. Rojo, J. M., Ojeda, G., Portoles, M. P. & Portoles, A. Inhibition of T and B lymphoblastic response by mithramycin, dacabazine, prospidium chloride and peptichemio. *Chemotherapy* **29**, 345–351 (1983).
12. Perez-Lopez, F. R., Urcia, M., Torralba, R., Lafarga, L. & Hergueta, L. Effect of prospidine administered at different times of the day on the development and growth of N-nitrosomethylurea-induced mammary tumors in Wistar rats. *Cancer Lett.* **24**, 111–118 (1984).
13. Benenson, E. V. & Timina, O. B. Prospidine versus methotrexate pulse in highly active rheumatoid arthritis: A controlled 6-month clinical trial. *Clin. Rheumatol.* **13**, 54–59 (1994).
14. National Center for Biotechnology Information. PubChem Database. Prospidium chloride, CID=31937. https://pubchem.ncbi.nlm.nih.gov/compound/Prospidium-chloride. Accessed 31 Oct. 2019.
15. Haddad, S. *et al.* Regio- and stereoselective synthesis of spiropyrrolizidines and piperazines through azomethine ylide cycloaddition reaction. *J. Org. Chem.* **80**, 9064–9075 (2015).
16. Lee, H. X. *et al.* Regio- and stereoselective synthesis of dispiropyrrolizidines through 1,3-dipolar cycloaddition reaction: Inhibition of KRAS expression. *J. Mol. Struct.* **1263**, 133177 (2022).
17. Hendzel, M. J. *et al.* Mitosis-specific phosphorylation of histone H3 initiates primarily within pericentromeric heterochromatin during G2 and spreads in an ordered fashion coincident with mitotic chromosome condensation. *Chromosoma* **106**, 348–360 (1997).
18. Huang, Y. *et al.* The kinetics of G2 and M transitions regulated by B cyclins. *PLoS One* **8**, e80861 (2013).
19. Hayward, D. *et al.* Orchestration of the spindle assembly checkpoint by CDK1-cyclin B1. *FEBS Lett.* **593**, 2889–2907 (2019).
20. Minshull, J. *et al.* The A- and B-type cyclin associated cdc2 kinases in *Xenopus* turn on and off at different times in the cell cycle. *EMBO J.* **9**, 2865–2875 (1990).
21. Hwang, A. *et al.* Cell cycle-dependent regulation of the Cyclin B1 promoter. *J. Biol. Chem.* **270**, 28419–28424 (1995).
22. Steinmetz, M. O. & Prota, A. E. Microtubule-targeting agents: Strategies to hijack the cytoskeleton. *Trends Cell Biol.* **28**, 776–792 (2018).
23. Wordeman, L. & Vicente, J. J. Microtubule-targeting agents in disease: Classic drugs, novel roles. *Cancers* **13**, 5650 (2021).
24. Nakamura, Y. & Ishigaki, Y. Immunostaining and time-lapse analysis of Vinblastine-induced paracrystal formation in human A549 cells. *Oncol. Lett.* **8**, 2387–2392 (2014).
25. Gillis, A. D. *et al.* $p21^{Cip1/WAF1}$ mediates cyclin B1 degradation in response to DNA damage. *Cell Cycle* **8**, 253–256 (2009).
26. Lehle, S. *et al.* LORD-Q: A long-run real-time PCR-based DNA-damage quantification method for nuclear and mitochondrial genome analysis. *Nucleic Acids Res.* **42**, e41 (2014).
27. Soni, D. V. *et al.* Cyclin B1 is rate limiting but not essential for mitotic entry and progression in mammalian somatic cells. *Cell Cycle* **7**, 1285–1300 (2008).
28. Pines, J. & Hunter, T. Human cyclins A and B1 are differentially located in the cell and undergo cell cycle-dependent nuclear transport. *J. Cell. Biol.* **115**, 1–17 (1991).

29. Bentley, A. M. *et al.* Distinct sequence elements of cyclin B1 promote localization to chromatin, centrosomes and kinetochores during mitosis. *Mol. Biol. Cell.* **18**, 4847–4858 (2007).
30. Nakayama, Y. & Yamaguchi, N. Role of cyclin B1 levels in DNA damage and DNA damage-induced senescence. *Int. Rev. Cell Mol. Biol.* **305**, 303–337 (2013).
31. Kikuchi, I. *et al.* A decrease in cyclin B1 levels leads to polyploidization in DNA damage-induced senescence. *Cell Biol. Int.* **34**, 645–653 (2014).
32. Fung, H. & Demple, B. Distinct roles of Ape1 protein in the repair of DNA damage induced by ionizing radiation or bleomycin. *J. Biol. Chem.* **286**, 4968–4977 (2011).
33. Zhang, J. *et al.* Necrosis, and then stress induced necrosis-like cell death, but not apoptosis, should be the preferred cell death mode for chemotherapy: Clearance of a few misconceptions. *Oncoscience* **1**, 407–422 (2014).
34. Snyder, A. G. *et al.* Intratumoral activation of the necroptotic pathway components RIPK1 and RIPK3 potentiates antitumor immunity. *Sci. Immunol.* **4**, 2004 (2019).
35. Costa, F. B. *et al.* The novel piperazine-containing compound LQFM018: Necroptosis cell death mechanisms, dopamine D4 receptor binding and toxicological assessment. *Biomed. Pharmacother.* **102**, 481–493 (2018).
36. Chan, F.K.-M. *et al.* A role for tumor necrosis factor receptor-2 and receptor-interacting protein in programmed necrosis and antiviral responses. *J. Biol. Chem.* **278**, 51613–51621 (2003).
37. Strillic, B. *et al.* Tumour-cell-induced endothelial cells necroptosis via cell death receptor 6 promotes metastasis. *Nature* **536**, 215–218 (2016).
38. Sheldrick, G. M. Crystal structure refinement with SHELXL. *Acta. Cryst.* **C71**, 3–8 (2015).
39. Bourhis, L. J., Dolomanov, O. V., Gildea, R. J., Howard, J. A. K. & Puschmann, H. The anatomy of a comprehensive constrained, restrained refinement program for the modern computing environment–Olex2 dissected. *Acta Crystallogr. A Found Adv.* **71**, 59–75 (2015).
40. Barad, A. *et al.* Anti-proliferative activity of a purified polysaccharide isolated from the basidiomycete fungus *Paxillus involutus*. *Carbohydr. Polym.* **181**, 923–930 (2018).
41. Barnes, M. *et al.* Molecular insights into the coding region determinant-binding protein-RNA interaction through site-directed mutagenesis in the heterogeneous nuclear ribonucleoprotein-K-homology domains. *J. Biol. Chem.* **290**, 625–639 (2015).
42. Dannenmann, B. *et al.* Simultaneous quantification of DNA damage and mitochondrial copy number by long-run DNA-damage quantification (LORD-Q). *Oncotarget* **8**, 112417–112425 (2017).

Acknowledgements

This project was supported by funding from the NSERC Discovery Grant (227158) to CHL, the Canada Foundation for Innovation (34711) to CHL, and the BC Knowledge Development Fund (103970) to CHL. VL, MZ and JL were supported by UNBC Research Project Awards.

Author contributions

V.P.L., W.M.L. and C.H.L. conceptualized and designed the study. V.P.L. conducted the synthesis and experiments to prepare Figs. 1, 3, 4, 6 and Figs. S1–S11. W.M.L conducted the experiments and prepared Figs. 5, 7 and 8. B.O.P. conducted the X-ray crystallography experiments and prepared Fig. S11. V.L., J.L. and C.H.L. conducted the MTT assays and prepared Fig. 2 and Table 1. M.Z. conducted some of the flow cytometry experiments and prepared Fig. 6. C.H.L., W.M.L. and T.M.B. provided the supervision. C.H.L. wrote the first draft of the manuscript and managed manuscript revisions. C.H.L. provided funding and research facilities. All authors reviewed and approved the final manuscript.

Competing interests

The authors declare no competing interests.

Additional information

Supplementary Information The online version contains supplementary material available at https://doi.org/10.1038/s41598-023-35927-6.

Correspondence and requests for materials should be addressed to C.H.L.

Reprints and permissions information is available at www.nature.com/reprints.

Publisher's note Springer Nature remains neutral with regard to jurisdictional claims in published maps and institutional affiliations.